The Astrophysical Journal Letters, 870:L20 (6pp), 2019 January 10 https://doi.org/10.3847/2041-8213/aaf73a

Magnetically Inspired Explosive Outflows from Neutron-star Mergers

Antonios Nathanail[1], Oliver Porth[1,2], and Luciano Rezzolla[1]
[1] Institut für Theoretische Physik, Max-von-Laue-Strasse 1, D-60438 Frankfurt, Germany
[2] Astronomical Institute Anton Pannekoek, University of Amsterdam, Science Park 904, 1098 XH, Amsterdam, The Netherlands
Received 2018 October 23; revised 2018 December 4; accepted 2018 December 10; published 2019 January 10

Abstract

Binary neutron-star mergers have long been associated with short-duration gamma-ray bursts (GRBs). This connection was confirmed with the first coincident detection of gravitational waves together with electromagnetic radiation from GW170817. The basic paradigm for short-duration GRBs includes an ultra-relativistic jet, but the low-luminosity prompt emission together with follow-up radio and X-ray observations have hinted that this picture may be different in the case of GW170817. In particular, it has been proposed that large amounts of the magnetic energy that is amplified after the merger, can be released when the remnant collapses to a black hole, giving rise to a quasi-spherical explosion impacting on the merger ejecta. Through numerical simulations we investigate this scenario for a range of viewing angles, injected energies and matter densities at the time of the collapse. Depending on the magnitude of the energy injection and the remnant density, we find two types of outflows: one with a narrow relativistic core and one with a wide-angle, but mildly relativistic outflow. Furthermore, very wide outflows are possible, but require energy releases in excess of 10^{52} erg.

Key words: gamma-ray burst: general – relativistic processes

1. Introduction

The coincident and follow-up observations across the electromagnetic spectrum of the gravitational waves from the event GW170817 (Abbott et al. 2017a, 2017b) have introduced a new era for the study of dense matter. The detection of GRB 170817A, i.e., the electromagnetic counterpart to GW170817, has established the connection between binary neutron-star (BNS) mergers and short gamma-ray bursts (GRBs). Models have predicted such a connection through the production of a jet following the merger (Eichler et al. 1989; Narayan et al. 1992; Rezzolla et al. 2011).

GRB 170817A was a subluminous event suggesting that we were possibly not looking straight into a jet (Goldstein et al. 2017; Savchenko et al. 2017). The prompt emission alone could not give a clear picture of whether this is intrinsic or due to other factors, one possibility being the large observing angle with respect to the axis of the outflow that produced the emission. Furthermore, the first radio and X-ray afterglow detection tens of days after merger, could not clarify the picture (Hallinan et al. 2017; Margutti et al. 2017; Troja et al. 2017). Subsequent radio and X-ray observations have provided important clues, but it is still difficult to clearly distinguish between different models for the emission (Alexander et al. 2017, 2018; D'Avanzo et al. 2018; Dobie et al. 2018; Margutti et al. 2018; Mooley et al. 2018c; Nynka et al. 2018; Troja et al. 2018). A hundred days after the main event, the radio flux was still rising and showed that the outflow has somehow a radial and/or angular structure. However, the most recent observations favor a rather collimated outflow that possess a relativistic core with an opening angle $<5^\circ$ (Mooley et al. 2018a, 2018b).

Some of the proposed scenarios invoke the successful launch of a relativistic jet; however, it is not seen directly and only the cocoon is visible. Another possibility is that the jet may not break out from the BNS ejecta, but merely deposit its energy there. Detailed discussions on models discussing either off-axis radiation from a jet or the cocoon emission from a choked jet have been presented by Murguia-Berthier et al. (2016, 2017), Lazzati et al. (2017), Gottlieb et al. (2018), Bromberg et al. (2018), Kathirgamaraju et al. (2018), Hotokezaka et al. (2018), Xie et al. (2018), and Salafia et al. (2018).

General-relativistic simulations have recently drawn a robust picture of BNS mergers, showing that mass ejection can be significant during merger, from which a visible kilonova is produced due to *r*-processes. The standard short-GRB picture envisions a jet to be produced after the collapse to a black hole of the merger remnant. If a jet was produced in GRB 170817A, its interaction with the ejecta is probably at the heart of the phenomenology observed.

Despite the differences in the numerous proposed models, a shared featured is the assumption that shortly after merger the remnant collapses to a black hole (Granot et al. 2017; Margalit & Metzger 2017; Shibata et al. 2017; Metzger et al. 2018; Nathanail 2018; Rezzolla et al. 2018). In this paper we describe a different possibility that naturally gives rise to two families of outflows following the merger: one with a narrow relativistic core and one with a wide-angle, mildly relativistic outflow. More specifically, depending on the collapse time and properties of the surrounding matter, we show that a jet need not be launched (Lehner et al. 2012; Nathanail 2018). However, the collapse of the remnant could initiate an "explosion," namely, a sudden release of large amounts of the magnetic energy that was amplified via instabilities during the early stages of the merger, and that can reach values even in excess of 10^{51} erg (Kiuchi et al. 2018). When this energy is released, it can push and accelerate the material in the vicinity of the compact remnant. This accelerated material will not be able to propagate through the high-density torus, which is mostly concentrated on the binary orbital plane. Simulations also show that the density of the material around the compact remnant has a strong angular dependence, being considerably smaller toward the orbital axis (Bovard et al. 2017). As a result, the produced outflow has a natural "escape route" along the polar direction, where it can propagate essentially freely and where, when accelerated, can quickly catch up to the slow-moving ejecta (Rezzolla & Kumar 2015).

Several hydrodynamic simulations in multidimensions have modeled an injected outflow that passes through the BNS ejecta (Lazzati et al. 2017; Murguia-Berthier et al. 2017; Gottlieb et al. 2018; Kathirgamaraju et al. 2018; Xie et al. 2018). Here, on the other hand, the outflow is the product of a single spherical energy release (explosion) triggered by the collapse of the compact remnant. Hence, all of the energy is injected at one instant in time and not continuously; this represents an important difference with respect to previous work and leads, indeed, to novel features.

In particular, we investigate such a scenario through general-relativistic two-dimensional simulations where the BNS ejecta are described in terms of a torus whose size and density profile depend on the time when the compact remnant of the merger collapses to a black hole, with the the maximum density of the torus $\rho_{\rm tor}$ decreasing as the time of collapse $t_{\rm coll}$ is increased. We then vary the amount of energy injected at the time of collapse in the range of 10^{48}–10^{52} erg and find that the energy injection leads quite robustly to either a wide-angle, mildly relativistic outflow or an outflow with a relativistic and narrow core. Note that while an "unsuccessful jet" normally refers to a jet that is produced but cannot emerge through the BNS ejecta, a jet is never produced in our study.

Particular attention should be paid to our models `E.50.9` and `E.51.10` which have a faster-moving core in a cone $\lesssim 10^{\circ}$ and reach $\Gamma \gtrsim 10$ (models `E.51.9` and `E.52.10` have also a faster-moving core, but a slightly different energy distribution). These properties make them compatible with the observational constraints reported in Mooley et al. (2018a), who argue that the emission around the peak of the lightcurve come from a component with angular extent $\lesssim 14^{\circ}$ and $\Gamma \simeq 4$. Furthermore, because of the faster-moving core, these models should naturally lead to a steep post-peak decay, again in agreement with the interpretations of Mooley et al. (2018b).

2. Numerical Setup

We employ `BHAC` to solve the relativistic-hydrodynamic equations in a Kerr background spacetime (Porth et al. 2017). The initial setup is chosen to resemble the ejected matter and the expanded torus around the compact remnant that formed during the BNS merger. Our simulations are performed in two spatial dimensions exploiting the approximate azimuthal symmetry of the system and we take advantage of three levels of mesh refinement to resolve the outflow at an effective resolution of 2048×512 cells (the radial grid has a logarithmic spacing with a minimum size of 40 m). We initialize the fluid with an equilibrium torus with constant specific angular momentum (Fishbone & Moncrief 1976) around a Kerr black hole with $M \sim 2.7\,M_{\odot}$ and a dimensionless spin of $a := J/M^2 = 0.93$; although the latter is somewhat larger than what is expected, the precise value used for the angular momentum J has little influence on our results because the energy injection is extremely rapid and most of the fluid dynamics takes place far from the black hole. The torus has a size of 1200 km and is contained in domain of radius 10,000 km.

The parameters of the torus are chosen after considering that the remnant of GW170817 must have survived $\lesssim 1$ s (Granot et al. 2017; Margalit & Metzger 2017; Shibata et al. 2017; Nathanail 2018; Rezzolla et al. 2018). Simulations indicate that after its formation, the torus around the compact remnant loses mass due to accretion, dynamical ejection via shock heating, and the emission of winds driven either by magnetic fields or neutrinos. All of these processes lead to redistribution of angular momentum, which is generically transported outward (Rezzolla et al. 2010). Hence, the mass and the maximum density of the torus must decreases over time leading us to initial configurations with maximum densities of $\rho_{\rm tor} \simeq 10^{11}$, 10^{10}, 10^{9} g cm^{-3}, thus corresponding to collapse times of $t_{\rm coll} \simeq$ 0.5, 1.0, 2.0 s, respectively; these values match well the results of numerical simulations (Bovard et al. 2017; Fujibayashi et al. 2018).

Table 1
Properties of the Various Scenarios Considered: Energy Released at Collapse $E_{\rm exp}$, Maximum Density of the Torus $\rho_{\rm tor}$, Time of Collapse $t_{\rm coll}$, Average Lorentz Factor $\langle\Gamma\rangle$, Averaged Lorentz Factor $\langle\Gamma\rangle_{30}$ within 30° from the Polar Axis, and the Outflow Mass Moving with $\Gamma > 1.2$

Model	$E_{\rm exp}$ (erg)	$\rho_{\rm tor}$ (g cm^{-3})	$t_{\rm coll}$ (s)	$\langle\Gamma\rangle$	$\langle\Gamma\rangle_{30}$	$M_{(\Gamma>1.2)}$ ($10^{-7}\,M_{\odot}$)
`E.50.11`	10^{50}	10^{11}	0.5	1.10	1.21	6
`E.51.11`	10^{51}	10^{11}	0.5	1.50	2.48	90
`E.52.11`	10^{52}	10^{11}	0.5	2.53	5.57	630
`E.49.10`	10^{49}	10^{10}	1.0	1.10	1.21	0.6
`E.50.10`	10^{50}	10^{10}	1.0	1.50	2.48	9
`E.51.10`	10^{51}	10^{10}	1.0	2.53	5.57	63
`E.52.10`	10^{52}	10^{10}	1.0	2.39	4.47	1400
`E.48.09`	10^{48}	10^{9}	2.0	1.10	1.21	0.06
`E.49.09`	10^{49}	10^{9}	2.0	1.50	2.48	0.9
`E.50.09`	10^{50}	10^{9}	2.0	2.53	5.57	6.3
`E.51.09`	10^{51}	10^{9}	2.0	2.39	4.47	140
`E.52.09`	10^{52}	10^{9}	2.0	3.26	4.55	3000

In a BNS merger, the region near the polar axis is filled with ejected matter, although at lower densities than near the equatorial plane. To reproduce these conditions together with the use of non-self-gravitating equilibrium tori, we also fill this region with matter, as it has a density that is two and a half orders of magnitude smaller than the maximum density in the equilibrium torus and has a radial fall-off that scales as $r^{-1.5}$, with r being the radial distance from the black hole. Overall, in our simulations the integrated rest-mass outside the black hole is $M_{\rm tor} = 6 \times 10^{-2}\,M_{\odot}$ and $M_{\rm ej} = 1 \times 10^{-2}\,M_{\odot}$. Since the ejected matter is moving outward with an average velocity of $\langle\beta\rangle := \langle\, v\,\rangle/c \sim 0.2$–$0.3$ (Foucart et al. 2016; Lehner et al. 2016; Radice et al. 2016, 2018; Sekiguchi et al. 2016; Bovard et al. 2017), and this is considerably slower than the relativistic outflow produced by the explosion. Initially, the matter in/outside the torus is set to have an azimuthal/zero velocity only.

Finally, the amount of energy released needs to be specified. Although studies of the energetics of collapsing isolated neutron stars exist (Most et al. 2018), the amount of energy available is still unclear. Numerous numerical simulations have shown that magnetic energy can be amplified after the merger due to instabilities either at the shear layer between the two neutron stars or in the bulk of the remnant. All in all, the magnetic energy can reach values as high as 10^{51} erg (Kiuchi et al. 2018) and even higher values are thought possible. At the time of collapse of the remnant, most of this magnetic energy is released almost isotropically and generates a strong shock with the external matter. In our simulations, which are purely hydrodynamical, we assume that all of this energy is released in the form of internal (thermal) energy that we inject at time $t = t_{\rm coll}$ by initializing an excess internal energy in a spherical shell between $r_{\rm in} \simeq 20$ km and $r_{\rm out} \simeq 23.8$ km, which is

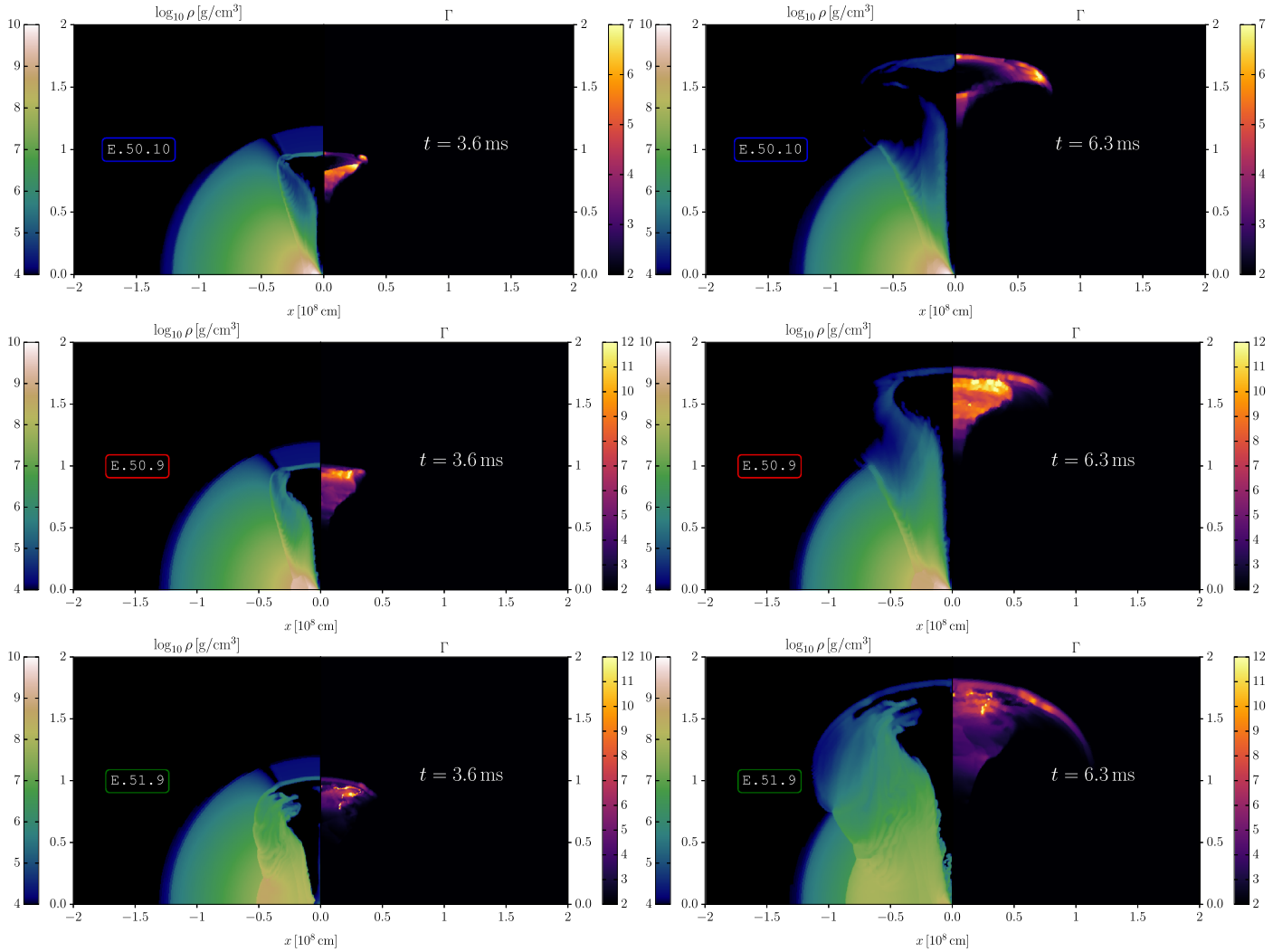

Figure 1. Top: density (left panels) and Lorentz factor (right panels) at two different times for an explosion of 10^{50} erg on a torus of maximum density 10^{10} g cm^{-3}, `E.50.10`. Middle and bottom: the same, but for `E.50.9` and `E.51.9`, respectively.

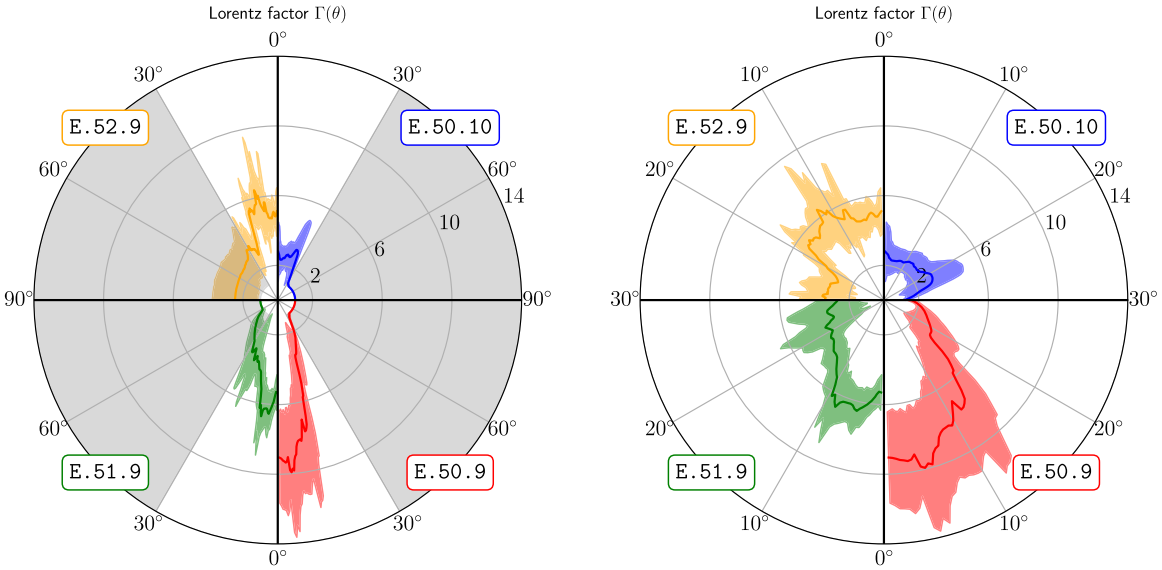

Figure 2. Polar plots of the Lorentz factor for four representative outflows over a quadrant (left panel), or within a cone of 30° (right panel); the thick lines show the average values, while the shaded region shows the 1σ variance.

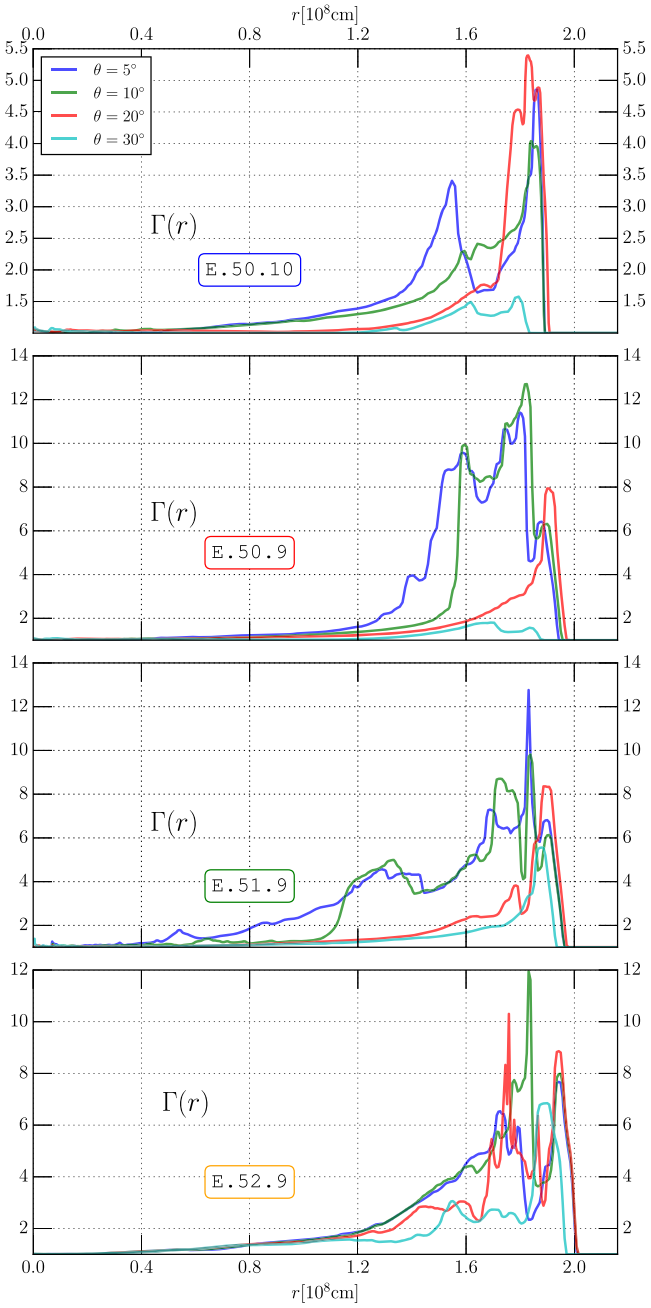

Figure 3. Radial dependence of the Lorentz factors; each plot shows $\Gamma(r)$ along polar slices at $\theta = 5°$, 10°, 20°, and 30°.

located between black hole and the torus inner edge. More precisely, if $E_{\rm exp}$ is the amount of energy released in a spherical shell of radii $r_{\rm in}$ and $r_{\rm out}$, we inject in the corresponding cells a pressure $p_{\rm sh} \propto 9\pi\, E_{\rm exp}/[\rho_{\rm tor}(r_{\rm in}^3 - r_{\rm out}^3)]$.

Although we neglect magnetic fields here, we also note that the large majority of the simulations of short-GRB jets discussed recently in the literature have been performed mostly in the hydrodynamic limit (Murguia-Berthier et al. 2016; Lazzati et al. 2017; Murguia-Berthier et al. 2017; Gottlieb et al. 2018; Xie et al. 2018), although some MHD investigations have also been performed (Bromberg et al. 2018; Kathirgamaraju et al. 2018). Because of the scale freedom in the test-fluid approximation, the ratio of the shell energy density to torus density is the only degree of freedom. Hence, increasing/decreasing the injected energy together with the density of the torus leaves the whole setup unchanged. This has the important advantage that only five simulations need to be performed to cover the 12 representative cases reported in Table 1.

3. Results

As the energy is injected at the center of the system, it produces a strong shock on the equatorial plane, which cannot break out because of the high-density material that it finds on its way. On the other hand, the less dense regions near the pole allow for matter to expand rapidly and then break out in a low-density region.

Rather quickly (see the top left panel of Figure 1), the shocked material in the polar region reaches Lorentz factors higher than five and acceleration is still ongoing. As time progresses, the shock piles up matter as it passes through the funnel leaving behind a very low-density region. In addition, the shock begins a sideways expansion as the outer parts of the ejected-matter distribution (i.e., the torus), decrease in density (see the top right panel of Figure 1). At a radius of ∼1200 km, the density has already fallen by almost six orders of magnitude, and can be taken as the break out radius of the outflow into the low-density region. As the energy released is increased (middle and bottom panels of Figure 1), it either is converted into kinetic energy of the outflow, which then acquires larger Lorentz factors (e.g., `E.50.9`), or disrupts the torus without a significant acceleration of the outflow (e.g., `E.51.9`).

Besides what is shown in Figure 1, the angular structure of the outflow can be best quantified through the polar plots in Figure 2, which report the Lorentz factors achieved as measured in slices of constant radius, i.e., $r \sim 2000$ km, and integrated over a time interval of $\tau_{\rm avg} \sim 1.8$ ms. More specifically, each panel refers in its four quadrants to four representative models, i.e., `E.50.10`, `E.50.9`, `E.51.9`, and `E.52.09`, each indicated with a thick line, while the shaded areas show the 1σ variance over $\tau_{\rm avg}$, i.e., the 68% variation of the Lorentz factor at each angle. Furthermore, while the left panel in Figure 2 shows the global angular structure, i.e., across all latitudes, the right panel zooms in on the polar region, i.e., with $0 \leqslant \theta \leqslant 30°$, so as to offer a more detailed representation of the structure of the outflows.

Starting from the upper-right quadrant of Figure 2, which still refers to `E.50.10`, it is easy to see that the Lorentz factor reaches peak values of $\Gamma \simeq 2$ at an angle of 15°–20°, which is significantly larger than the average in a cone $0 \lesssim \theta \lesssim 30°$. Increasing the energy by one order of magnitude, as in `E.50.9`, (lower-right quadrant), the average Lorentz factor increases significantly, reaching values $\Gamma \simeq 10$ near the polar axis, while being overall confined within an angle of 30°. As the energy is further increased by one order of magnitude, as in `E.51.9` (lower-left quadrant), there is enough energy released to accelerate large amounts of ejecta. As a result, the outflow has comparable bulk Lorentz factors, but is now propagating in a much wider funnel, which extends up to $\theta \lesssim 60°$. Finally, in the most extreme case of `E.52.9`, matter at essentially all latitudes, hence also the dense torus on the equatorial plane, is pushed away, acquiring Lorentz factors $\Gamma \sim 2$–6 at angles as large as $\theta \sim 90°$.

In addition to a complex angular structure, the outflow also develops a nontrivial radial stratification, reported in Figure 3,

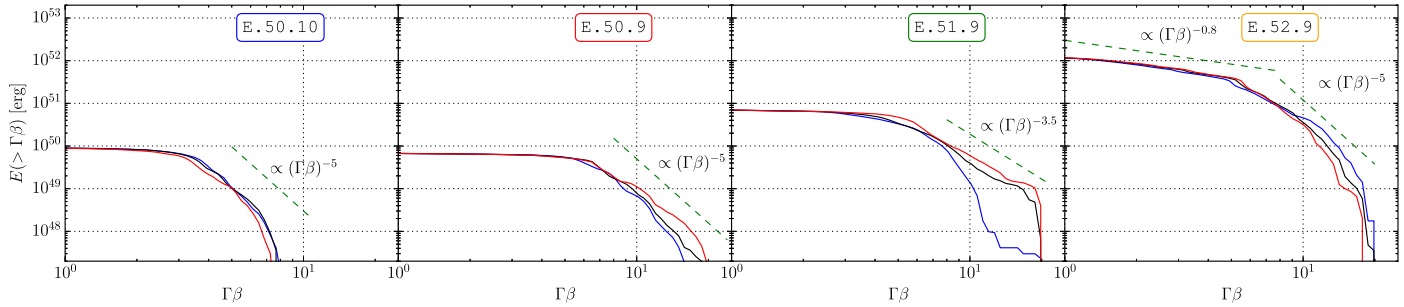

Figure 4. Energy structure for four representative outflows. The blue, black, and red solid lines represent the distribution at different times: $t = 6.6$, 8.0, and 9.3 ms, respectively.

where we show $\Gamma(r)$ at $t \sim 1.8$ ms in four different directions, i.e., $\theta = 5°$, 10°, 20°, and 30°. In all cases, and as expected in a spherical blast wave, the fast-moving parts of the outflow are those in the leading edge of the wave (Blandford & McKee 1976), which reach Lorentz factors of the order $\Gamma \sim 5$–10. At the same time, and in contrast to a standard blast wave, the velocity in the tail of the wave does not decrease monotonically, but shows secondary peaks that have comparable Lorentz factors (indeed even larger in the case of `E.50.10`), in particular within a cone of $\sim 10°$ from the polar axis. This complex stratification is due to multiple shock reflections in the low-density funnel and to a shear flow as the wave interacts with the denser torus material. Interestingly, the conditions reproduced here could lead to a tangential-velocity booster (Aloy & Rezzolla 2006), which develops when the dynamics of a relativistic jet can be assimilated to the motion of two fluids, the inner one being much hotter moving with a large tangential velocity with respect to the cold, slowly moving outer fluid. These conditions are often met in numerical simulations of short GRBs.

With the exception of the top one, all panels in Figure 3 have the same vertical scale and very comparable values of the Lorentz factor at least within an angle of $\theta \lesssim 20°$. Since the panels report injected energies differing by one order of magnitude (or more), this similarity indicates that as more energy is released, this is converted to accelerate larger portions of the ejecta rather than to further accelerate the material near the polar axis. This is an important finding pointing out that wide outflows require energy releases in excess of 10^{52} erg; of course, such a large amount of injected magnetic energy is rather unrealistic.

It is also interesting to note the similarities of the models described here with the properties of the outflows that can fit the late afterglow of GW170817. The latter can be explained in terms of a wide-angle outflow that is re-energized by slower parts of the flow following the first and fast-moving leading part. As the fast part of the flow starts moving into the interstellar medium (ISM) and decelerates, the slower parts catch up causing an increase in the afterglow flux (Troja et al. 2018).

Mooley et al. (2018c) have shown that the early radio-afterglow of GW170817 can be explained with a cumulative energy profile of $E(>\Gamma\beta) \propto (\Gamma\beta)^{-\alpha}$, where E is the sum of the internal and kinetic energy and $E(>\Gamma\beta)$ is the energy of the outflow in excess of $\Gamma\beta$; the observations suggest that $\alpha \simeq 5$. In Figure 4 we show the structure of the energy as a function of $\Gamma\beta$ for the four representative models. The energy is measured after the front part of the outflow has reached the low-density region and has been reported at three different times with a separation of 1.4 ms in time. As can be seen from Figure 4, the high-velocity tails of all flows indeed show a steep profile that scales nearly like $\propto(\Gamma\beta)^{-5}$; furthermore, the knee between the constant-energy distribution and the power law moves to larger values of $\Gamma\beta$ as the energy released is increased. Note also that in the exceptionally energetic model `E.52.9`, the slow part of the flow exhibits another power law with slope -0.8.

The shock produced from the interaction between the expanding outflow and the surrounding ISM emits multi-wavelength synchrotron radiation and is a helpful tool to distinguish between models (Nakar & Piran 2011). The afterglow of GW170817 indicated that there was an energy increase at the shock with the ISM either by a radial stratification of the flow (which is naturally developed in our models) or by the widening of the beaming cone of a relativistic jet, which gradually comes into our line of sight. Clearly, an important development of the results presented here will be represented by radiative-transfer calculations of the radiation produced as this outflow impacts the ISM and leaves a distinctive imprint, possibly in the degree of polarization, which could break the degeneracy among different possible models (Gill & Granot 2018).

4. Conclusions

We have performed a series of general-relativistic hydrodynamical simulations modeling a possible scenario accompanying the collapse of the remnant produced by a BNS merger. In particular, we have shown that if a spherical "explosion," namely, an isotropic and sudden release of magnetic energy is triggered around one second after the merger, a narrow outflow with a relativistic core or a wide-angle, mildly relativistic outflow is generated. The outflow propagates mostly through the polar regions, where the density is much smaller. Although only mildly relativistic, the outflow quickly catches-up with the far slower merger ejecta, breaking-out in the low-density region where it acquires a wide angular structure. Since our initial energy injection is perfectly isotropic, the final angular distribution of the outflow and its radial stratification are the consequence of the propagation through the highly anisotropic distribution of the ejecta. Interestingly, the outflow develops an energy dependence close to $\propto\Gamma\beta^{-5}$, in an encouraging agreement with the recent radiative models of the early afterglow of Mooley et al. (2018c).

While this work is meant as the exploration of a plausible scenario for GRB 170817A, several future improvements can be made. First, while axisymmetry is probably a good approximation, it is important to validate these results with three-dimensional simulations. Second, magnetic fields will be present inside and outside of the merger remnant and with a complex topology (Siegel et al. 2014). The interaction of the

ejecta with these magnetic fields needs to be taken into account with MHD simulations. Third, when the black hole is formed, it will ring down, producing pulses of electromagnetic radiation (Most et al. 2018), possibly impacting the stratification of the outflow. Finally, we note that our model should not be seen as being in contrast with the standard jet-formation scenario in short GRBs. Rather, it argues that not all BNS mergers can produce a jet and shows that even without the production of a collimated jet, a mildly relativistic outflow can be expected if sufficient magnetic energy is released when the remnant collapses.

It is a pleasure to thank D. Giannios and R. Gill for useful discussions. A.N. is supported by a von-Humboldt Fellowship. Support also comes from the ERC synergy grant "BlackHoleCam: Imaging the Event Horizon of Black Holes" (grant No. 610058), "PHAROS," COST Action CA16214; the LOEWE-Program in HIC for FAIR; the European Union's Horizon 2020 Research and Innovation Programme (Grant 671698) (call FETHPC-1-2014, project ExaHyPE). The simulations were performed on the clusters SuperMUC (LRZ, Garching), LOEWE (CSC, Frankfurt), and HazelHen (HLRS, Stuttgart).

ORCID iDs

Luciano Rezzolla https://orcid.org/0000-0002-1330-7103

References

Abbott, B. P., Abbott, R., Abbott, T. D., et al. 2017a, PhRvL, 119, 161101
Abbott, B. P., Abbott, R., Abbott, T. D., et al. 2017b, ApJL, 848, L12
Alexander, K. D., Berger, E., Fong, W., et al. 2017, ApJL, 848, L21
Alexander, K. D., Margutti, R., Blanchard, P. K., et al. 2018, ApJL, 863, L18
Aloy, M. A., & Rezzolla, L. 2006, ApJL, 640, L115
Blandford, R. D., & McKee, C. F. 1976, PhFl, 19, 1130
Bovard, L., Martin, D., Guercilena, F., et al. 2017, PhRvD, 96, 124005
Bromberg, O., Tchekhovskoy, A., Gottlieb, O., Nakar, E., & Piran, T. 2018, MNRAS, 475, 2971
D'Avanzo, P., Campana, S., Salafia, O. S., et al. 2018, A&A, 613, L1
Dobie, D., Kaplan, D. L., Murphy, T., et al. 2018, ApJL, 858, L15
Eichler, D., Livio, M., Piran, T., & Schramm, D. N. 1989, Natur, 340, 126
Fishbone, L. G., & Moncrief, V. 1976, ApJ, 207, 962
Foucart, F., Haas, R., Duez, M. D., et al. 2016, PhRvD, 93, 044019
Fujibayashi, S., Kiuchi, K., Nishimura, N., Sekiguchi, Y., & Shibata, M. 2018, ApJ, 860, 64
Gill, R., & Granot, J. 2018, MNRAS, 478, 4128
Goldstein, A., Veres, P., Burns, E., et al. 2017, ApJL, 848, L14
Gottlieb, O., Nakar, E., & Piran, T. 2018, MNRAS, 473, 576
Granot, J., Guetta, D., & Gill, R. 2017, ApJL, 850, L24
Hallinan, G., Corsi, A., Mooley, K. P., et al. 2017, Sci, 358, 1579
Hotokezaka, K., Kiuchi, K., Shibata, M., Nakar, E., & Piran, T. 2018, ApJ, 867, 95
Kathirgamaraju, A., Barniol Duran, R., & Giannios, D. 2018, MNRAS, 473, L121
Kiuchi, K., Kyutoku, K., Sekiguchi, Y., & Shibata, M. 2018, PhRvD, 97, 124039
Lazzati, D., Deich, A., Morsony, B. J., & Workman, J. C. 2017, MNRAS, 471, 1652
Lehner, L., Liebling, S. L., Palenzuela, C., et al. 2016, CQGra, 33, 184002
Lehner, L., Palenzuela, C., Liebling, S. L., Thompson, C., & Hanna, C. 2012, PhRvD, 86, 104035
Margalit, B., & Metzger, B. D. 2017, ApJL, 850, L19
Margutti, R., Alexander, K. D., Xie, X., et al. 2018, ApJL, 856, L18
Margutti, R., Berger, E., Fong, W., et al. 2017, ApJL, 848, L20
Metzger, B. D., Thompson, T. A., & Quataert, E. 2018, ApJ, 856, 101
Mooley, K. P., Deller, A. T., Gottlieb, O., et al. 2018a, Natur, 561, 355
Mooley, K. P., Frail, D. A., Dobie, D., et al. 2018b, ApJL, 868, L11
Mooley, K. P., Nakar, E., Hotokezaka, K., et al. 2018c, Natur, 554, 207
Most, E. R., Nathanail, A., & Rezzolla, L. 2018, ApJ, 864, 117
Murguia-Berthier, A., Ramirez-Ruiz, E., Kilpatrick, C. D., et al. 2017, ApJL, 848, L34
Murguia-Berthier, A., Ramirez-Ruiz, E., Montes, G., et al. 2016, ApJL, 835, L34
Nakar, E., & Piran, T. 2011, Natur, 478, 82
Narayan, R., Paczynski, B., & Piran, T. 1992, ApJL, 395, L83
Nathanail, A. 2018, ApJ, 864, 4
Nynka, M., Ruan, J. J., Haggard, D., & Evans, P. A. 2018, ApJL, 862, L19
Porth, O., Olivares, H., Mizuno, Y., et al. 2017, ComAC, 4, 1
Radice, D., Galeazzi, F., Lippuner, J., et al. 2016, MNRAS, 460, 3255
Radice, D., Perego, A., Hotokezaka, K., et al. 2018, ApJ, 869, 130
Rezzolla, L., Baiotti, L., Giacomazzo, B., Link, D., & Font, J. A. 2010, CQGra, 27, 114105
Rezzolla, L., Giacomazzo, B., Baiotti, L., et al. 2011, ApJL, 732, L6
Rezzolla, L., & Kumar, P. 2015, ApJ, 802, 95
Rezzolla, L., Most, E. R., & Weih, L. R. 2018, ApJL, 852, L25
Salafia, O. S., Ghisellini, G., Ghirlanda, G., & Colpi, M. 2018, A&A, 619, 18
Savchenko, V., Ferrigno, C., Kuulkers, E., et al. 2017, ApJL, 848, L15
Sekiguchi, Y., Kiuchi, K., Kyutoku, K., Shibata, M., & Taniguchi, K. 2016, PhRvD, 93, 124046
Shibata, M., Fujibayashi, S., Hotokezaka, K., et al. 2017, PhRvD, 96, 123012
Siegel, D. M., Ciolfi, R., & Rezzolla, L. 2014, ApJL, 785, L6
Troja, E., Piro, L., Ryan, G., et al. 2018, MNRAS, 478, L18
Troja, E., Piro, L., van Eerten, H., et al. 2017, Natur, 551, 71
Xie, X., Zrake, J., & MacFadyen, A. 2018, ApJ, 863, 58